Supporting Information

ZIF/Co-C_3N_4 with enhanced electrocatalytic reduction of carbon dioxide activity by photoactivation process

Huihui Qi,[a §] Yunjie Zhou,[a §] Yi Li,[a] Fan Liao,[a] Zhenzhen Wang, [a] Xiao Wang,[a] Hui Huang,*[a] Mingwang Shao,[a] Yang Liu *[a] and Zhenhui Kang *[a,b]

[a] Institute of Functional Nano & Soft Materials (FUNSOM), Jiangsu Key Laboratory for Carbon-Based Functional Materials & Devices, Soochow University, 199 Ren'ai Road, Suzhou, 215123, China.

[b] Macao Institute of Materials Science and Engineering, Macau University of Science and Technology, Taipa 999078, Macau SAR, China

[§] These authors contributed equally to this work.

1. 1. Experimental Section

1.1 Materials

Zinc acetate ($Zn(CH_3COO)_2 \cdot 2H_2O$, 99.0%), zinc nitrate ($Zn(NO)_3 \cdot 6H_2O$, 2-methylimidazole (2-MeIM, 99%), cobalt chloride ($CoCl_2 \cdot 6H_2O$, 99.7%), sodium hydroxide (KOH, 85.0%), potassium bicarbonate ($KHCO_3$, 99.5%), and ethanol (EtOH, 99.8%) were purchased from Sinopharm Chemical Reagent Co. Ltd (China). Urea（99.7%）was purchased from meryer. These materials were used in this study without further purification. Nafion perfluorinated resin solution (5 wt%) was purchased from Adamas-Betas; Nafion 212 proton exchange membrane and Toray Carbon Paper (TGP-H-60) were purchased from Alfa Aesar. Milli-Q ultrapure water (Millipore, ≥18 MΩ/cm) was used throughout the work.

1.2 Characterization.

The surface morphology and elemental composition of the catalyst were characterized by SEM, TEM and EDX spectra. The SEM and TEM images were acquired from a FEI-Quanta 200 FEG scanning electron microscope and FEI-Tecnai F20 transmission electron microscope (200 kV). The crystal structure was performed by X-ray diffraction (XRD) using an X'Pert-ProMPD (Holand) D/max-γ AX-ray diffractometer with Cu Kα radiation (λ = 0.154 178 nm). X-ray photoelectron spectroscopy (XPS) was obtained by using a KRATOS Axis ultra-DLD X-ray photoelectron spectrometer with a monochromatized Mg Kα X-ray source (hν = 1283.3 eV). The CO_2 adsorption was determined by plotting the adsorption isotherm of CO_2 at 25 °C obtained using a Micromeritics ASAP 2050 instrument. The Fourier-transform infrared (FTIR) spectra of the samples were recorded on a Hyperion spectrophotometer (Bruker) in the scan range of 400–4000 cm^{-1} using a standard KBr pellet technique. Room temperature UV-vis absorption spectrum was carried out from a UV/VIS/NIR spectrophotometer (Lambda 750, Perkinelmer), which the wavelength range is 200–800 nm. The electrocatalytic activities were determined using a Model CHI 760C workstation (CH Instruments, Chenhua, Shanghai, China).

1.3 Product Analysis.

The analytical measurement of the product was carried out in a closed H-type quartz cell (Nafion 212 membrane). The catalyst (dissolved in 0.5 wt% Nafion) modified carbon fiber paper (1 cm × 2 cm) was used as the working electrode. CO_2 saturated 0.5M $KHCO_3$ was used as the electrolyte for the reaction. During the measurements, the working electrodes were irradiated by a Xe lamp equipped with an AM 1.5 filter. The carbon-containing gas products (CO, CH_4, C_2H_4, and C_2H_6) were tested using a flame ionization detector (FID) and a TDX-1 chromatographic column with a methane converter. The major by-product (H_2) was tested using a thermal conductivity detector (TCD) and a molecular sieve 5A packed column. The liquid phase products were studied using a Bruker Avance III 400 NMR spectrometer, in which 0.5 mL electrolyte was mixed with 0.1 mL D_2O (deuterated water) and 0.05 μL dimethyl sulfoxide (DMSO, Sigma, 99.99%) was added as an internal standard. The electrochemical test was performed under the same conditions except that the working electrode was not illuminated.

Faraday's efficiency is calculated as follows:

$FE(CO) =[z*n(CO)* F/Q] *100\%$

$FE(H_2) = [z*n(H_2)* F/Q] *100\%$

where z is the number of electrons exchanged; for example, z = 2 for reduction of CO2 to CO. F is the Faraday constant (F = 96485 C/ mol), n(CO) is the number of moles for produced CO, and

$n(H_2)$ is the number of moles for the produced H_2, which were measured by GC. Q is the total charge passed.

1.4 $KHCO_3$ concentration dependence

The $[HCO_3]$- dependence study was performed at a constant applied potential (-0.8 V *vs*. RHE under light and -1.0V *vs*. RHE in the darkness) at $KHCO_3$ concentrations varying from 0.3 to 0.9 M. KCl was added to the low $KHCO_3$ concentration solutions to maintain the same ionic strength**.**

1.5 *In-situ* transient photovoltage (TPV) measurements

The TPV measurements were conducted under room temperature on platinum net covered with power sample (1 cm×1 cm) as the working electrodes and Pt wire as the counter electrodes. The *in-situ* TPV test was carried out under room temperature with indium-tin oxide (ITO) glass (1 cm×2 cm) as the working electrodes and Pt wire as the counter electrodes. The working electrodes were prepared by depositing samples on ITO glass substrates. During the testing process, the working electrodes were kept wet with anhydrous acetonitrile (adding N_2, CO_2 saturated). The TPV was excited with a nanosecond laser radiation pulse (wavelength of 355 nm and the repetition rate was 5 Hz) from a third harmonic Nd:YAG laser (Beamtech Optronics Co., Ltd.). The TPV signals were amplied by an amplifier and were recorded by an oscilloscope. All measurements were performed at room temperature and under ambient pressure.

2 Additional figures

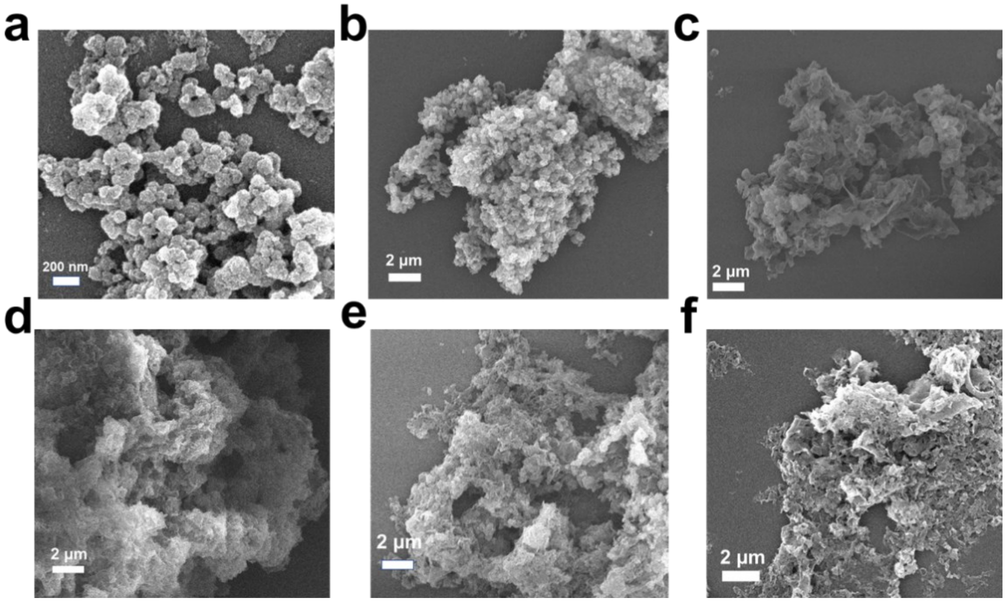

Figure. S1. SEM images of (a) ZIF-8-Co, (b) ZIF/Co, (c) C_3N_4, (d) ZIF/Co-C_3N_4-0.5%, (e) ZIF/Co-C_3N_4-1% and (f) ZIF/Co-C_3N_4-2%.

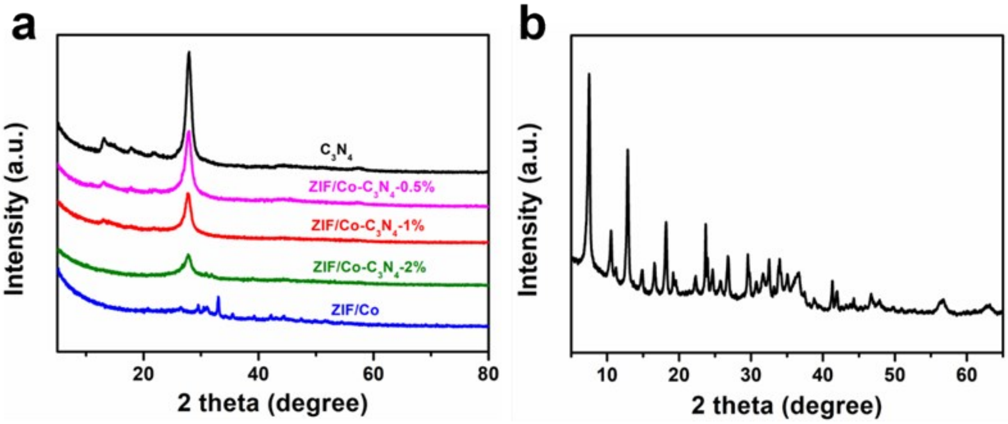

Figure. S2. XRD patterns of (a) ZIF/Co-C_3N_4 composite with different ZIF/Co contents (0.5 wt. %, 1 wt. % and 2 wt. %, respectively), C_3N_4 and ZIF/Co, and (b) ZIF-8-Co without fired in a tube furnace

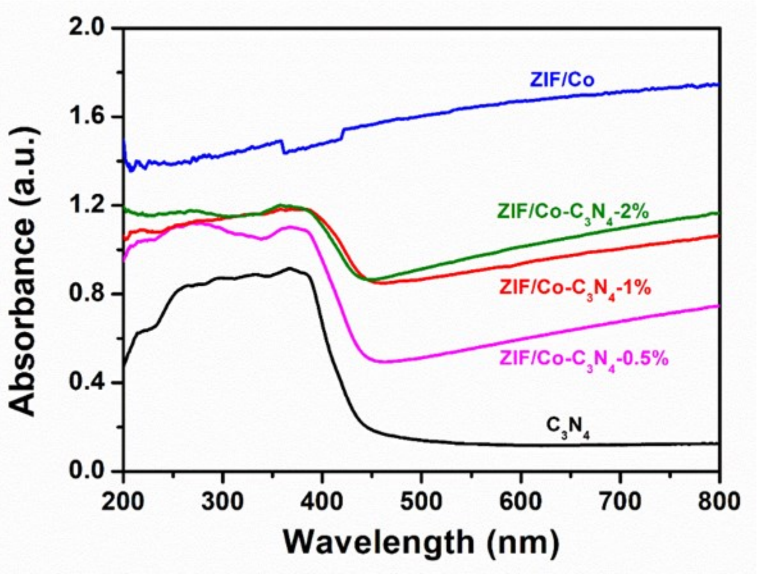

Figure. S3. UV-vis adsorption spectra of ZIF/Co-C_3N_4 composite with different ZIF/Co contents (0.5 wt. %, 1 wt. % and 2 wt. %, respectively), C_3N_4 and ZIF/Co.

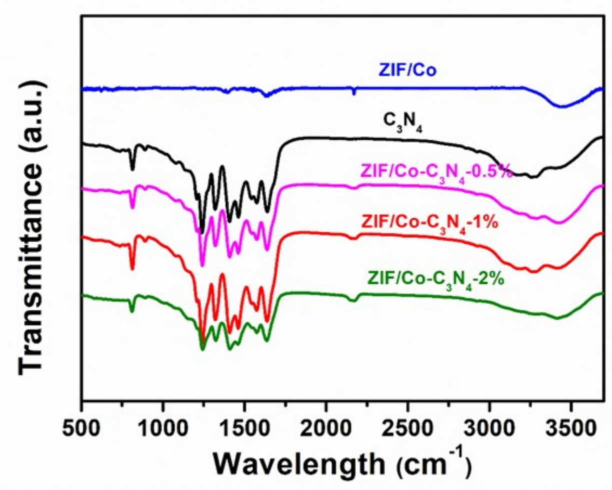

Figure. S4. FT-IR spectra of ZIF/Co-C_3N_4 composite with different ZIF/Co contents (0.5 wt. %, 1 wt. % and 2 wt. %, respectively), C_3N_4 and ZIF/Co.

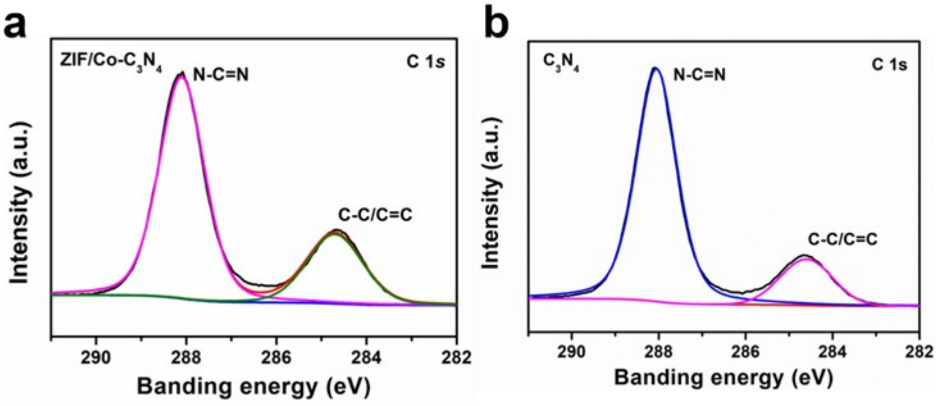

Figure. S5. High-resolution XPS spectra of C 1s for (a) ZIF/Co-C_3N_4 and (b) C_3N_4.

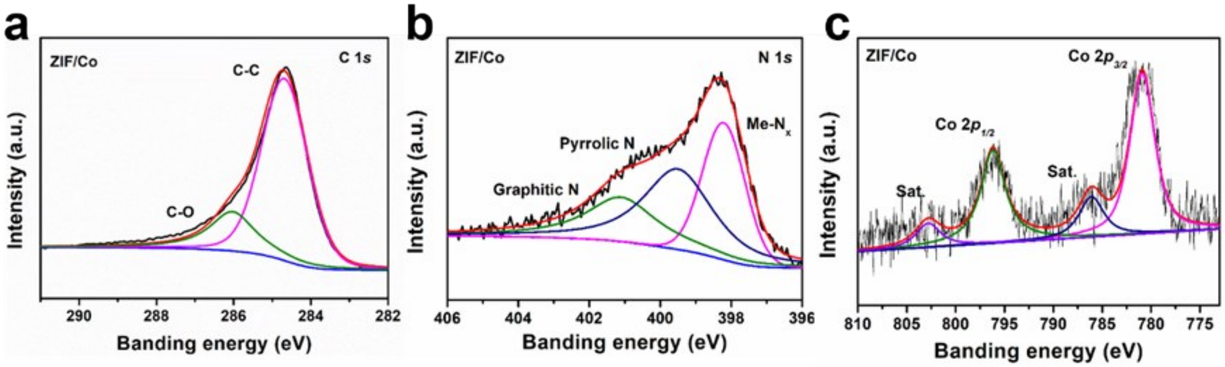

Figure. S6. High-resolution XPS spectra of (a) C 1s, (b) N 1s and (c) Co 2p for ZIF/Co-C_3N_4.

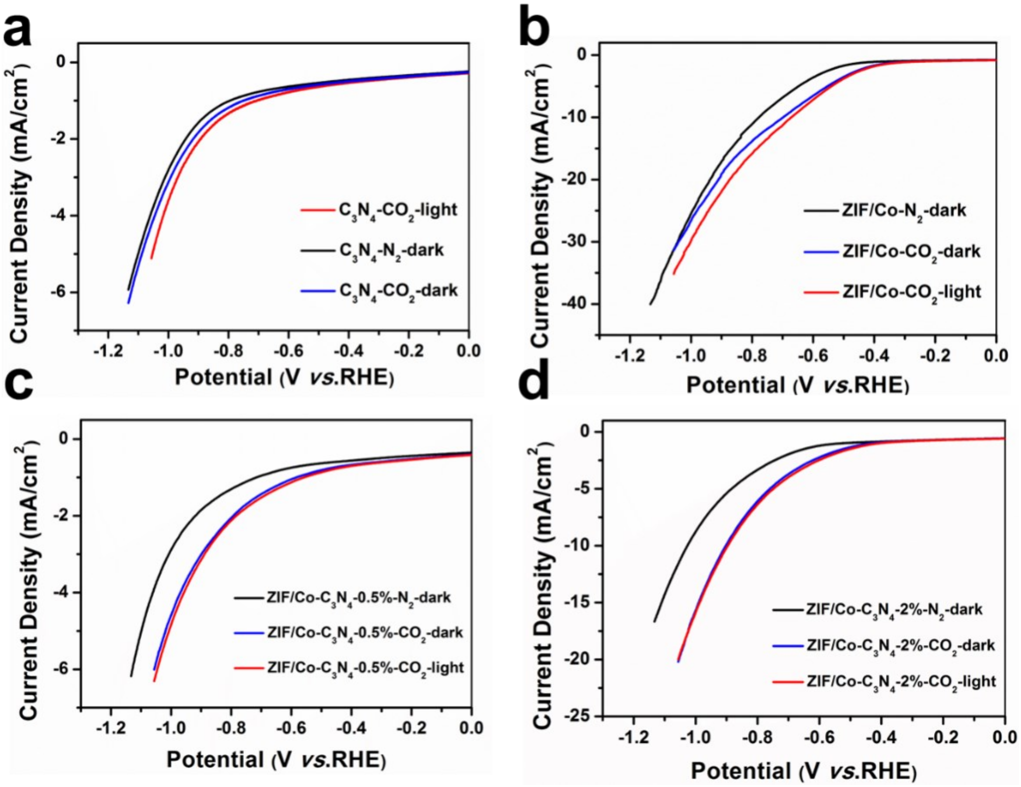

Figure. S7. LSV curves for (a) C_3N_4, (b)ZIF/Co, (c) ZIF/Co-C_3N_4-0.5%, (d) ZIF/Co-C_3N_4-2% in N_2-saturated (black trace), CO_2-saturated (blue trace) and CO_2-saturates with light radiation (red trace) in 0.5 M $KHCO_3$ electrolyte with a scan rate of 0.1 V s^{-1}.

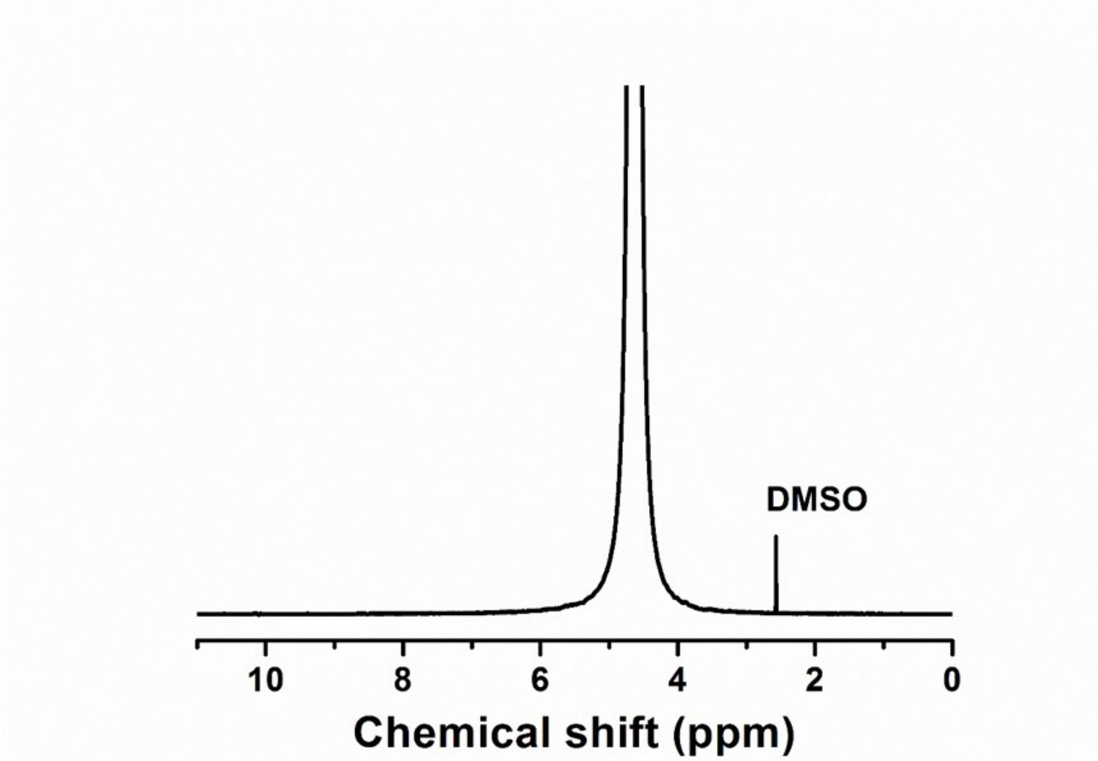

Figure. S8. Representative NMR spectrum of the electrolyte after CO_2 reduction electrolysis at -0.67 V *vs*. RHE under light.

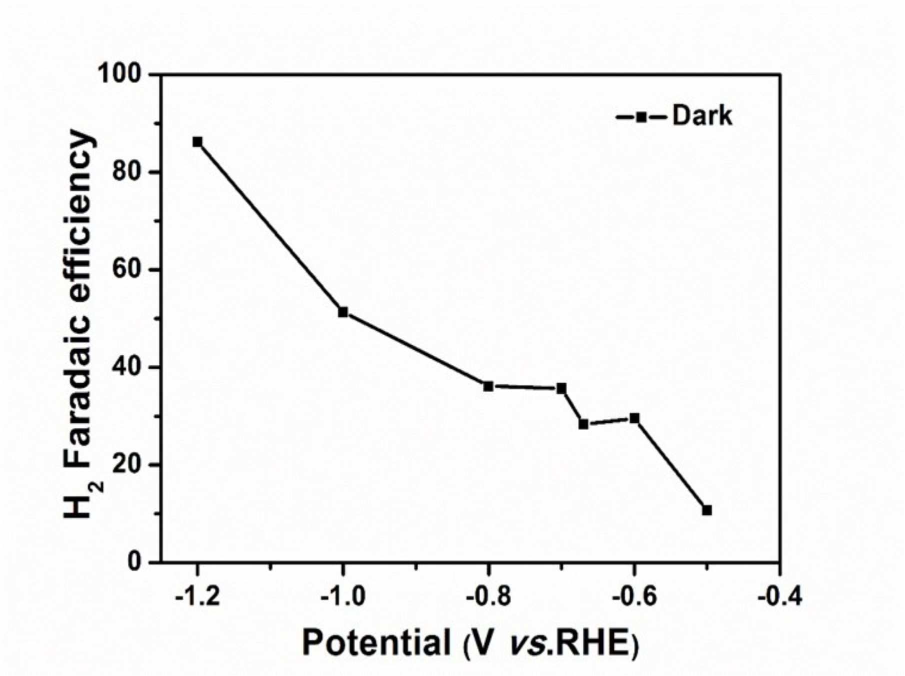

Figure. S9. Faradaic efficiency of H_2 of ZIF/Co-C_3N_4 in darkness.

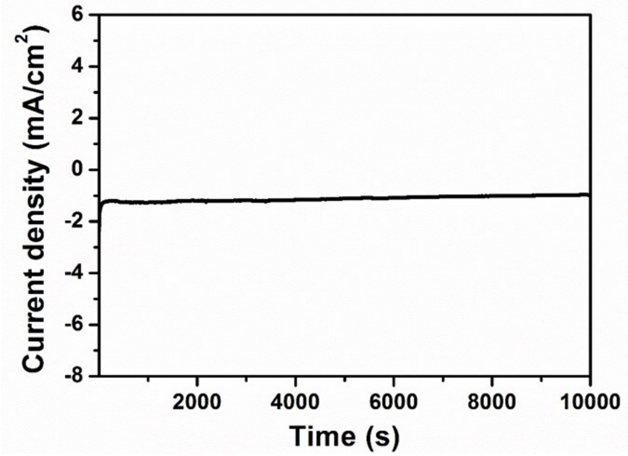

Figure. S10. Stability performance of ZIF/Co-C_3N_4 for CO_2 reduction operated at potentiostatic potential of −0.67 V *vs* RHE under light.

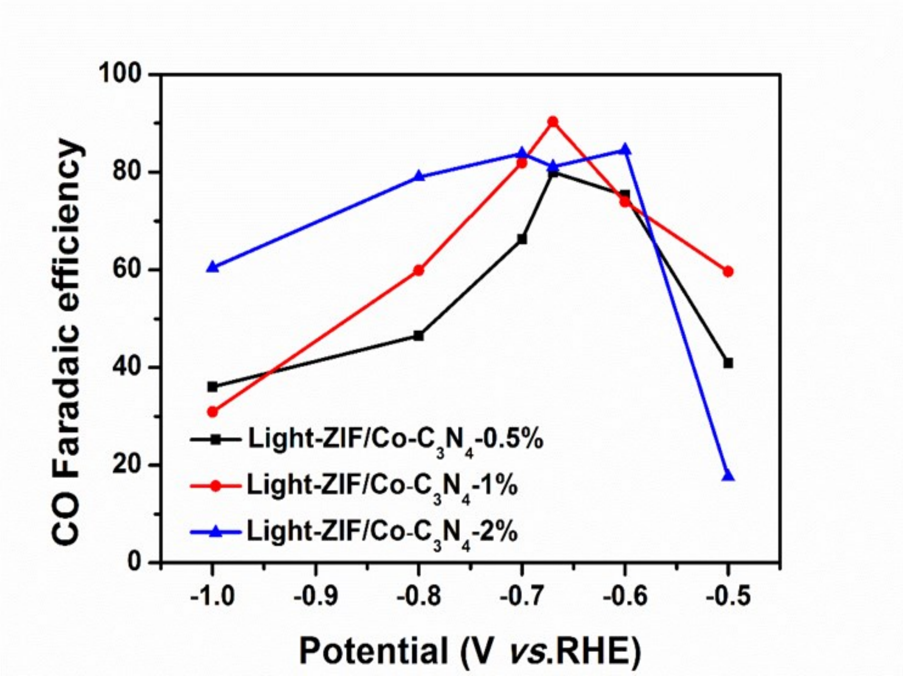

Figure. S11. The FEs of ZIF/Co-C_3N_4 composite with different ZIF/Co contents (0.5 wt. %, 1 wt. % and 2 wt. %).

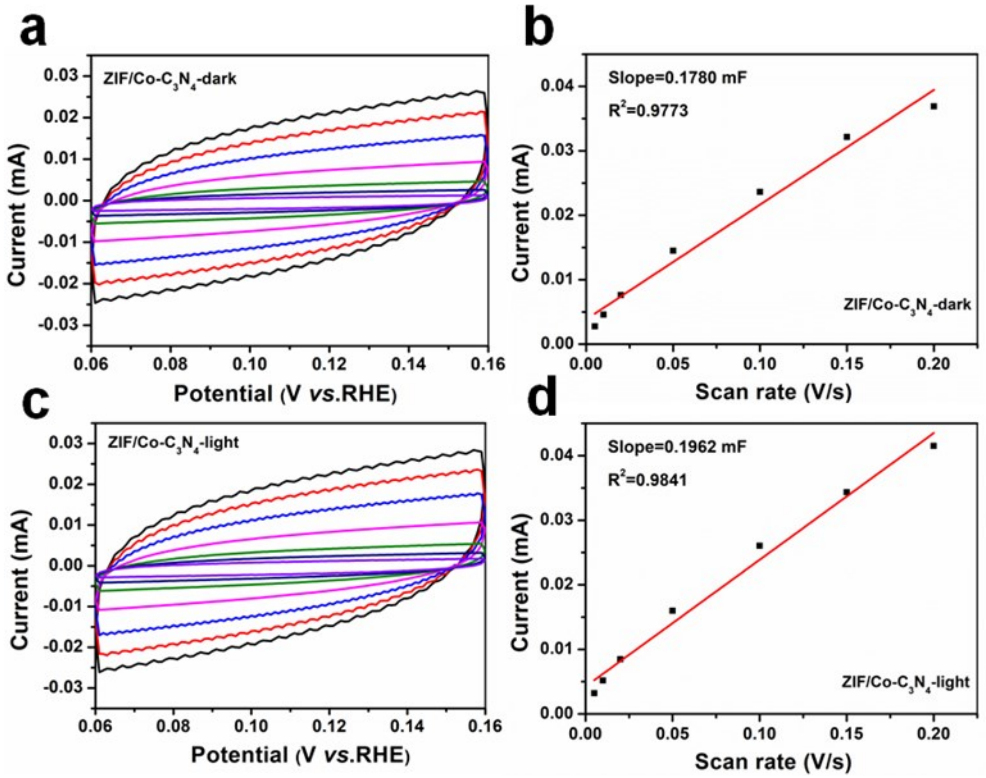

Figure. S12. Double-layer capacitances of ZIF/Co-C_3N_4 (a, b) in dark, (c, d) under light radiation.

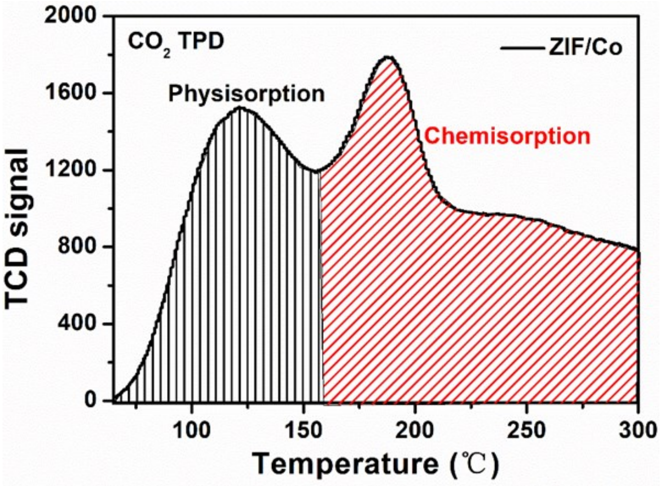

Figure. S13. CO_2-TPD curve of ZIF/Co.